Wu et al. Biochar (2026) 8:80
https://doi.org/10.1007/s42773-026-00592-1

Biochar

ORIGINAL RESEARCH Open Access

Green-synthesized iron nanoparticles enhance CMC/PVA coatings for biochar-zeolite slow-release fertilizers

Mengqiao Wu[1,2†], Zefeng Ruan[1,2†], Yuyuan Wu[1], Yang Cheng[1], Yuting Hong[1], Qinglin Gu[1], Yiting Zhang[1], Jialin Wei[1], Xiaowen Zhang[1], Chang Dong[1], Xu Zhao[1], Yongfu Li[1], Chengfang Song[1*] and Bing Yu[2*]

Abstract

The escalating demand for sustainable agriculture necessitates innovative slow-release fertilizers (SRFs) that enhance nutrient efficiency while mitigating environmental impacts. This study presents a new green-synthesized nano-iron (tea extract iron nanoparticles, T-FeNPs) reinforced carboxymethyl cellulose/polyvinyl alcohol (CMC/PVA) composite coating for zeolite–biochar hybrid SRFs. T-FeNPs were synthesized using tea extract as a reducing agent and incorporated into CMC/PVA matrices. The nanocomposite coatings were applied to fertilizer cores comprising zeolite, nitrogen-phosphorus-potassium (NPK) compound fertilizer, and rice straw biochar (RSBC). Soil leaching tests demonstrated superior nutrient retention: CMC/PVA/0.5Fe-SRF reduced cumulative N and P release to 58.47% and 15.82%, respectively, outperforming unmodified CMC/PVA-SRF and compound NPK fertilizers. Mechanistic investigation uncovered that physical barrier enhancement via pore obstruction by T-FeNPs significantly impedes water ingress and nutrient ion diffusion. In tomato cultivation, the CMC/PVA/0.5Fe-SRF treatment maximized plant height, biomass, and water retention, attributed to sustained nutrient release. Soil analysis revealed enhanced total N, P, K, cation exchange capacity, and organic matter content. Economic analysis indicated a production cost of $562.02/ton for CMC/PVA/0.5Fe-SRF, with potential global GHG reductions of 35.69 Mt CO_2e in East Asia alone via improved nitrogen use efficiency. Overall, this work presents a scalable, eco-friendly strategy for enhancing fertilizer efficiency and soil health.

Highlights

- T-FeNPs/CMC/PVA boosted biochar-based fertilizer's strength, hydrophobicity & controlled nutrient release.
- Optimal CMC/PVA/0.5Fe-SRF formulation reduced N/P leaching and boosted tomato growth and soil fertility.
- This technology offers substantial greenhouse gas reduction potential and costs an estimated 562.02 $ t^{-1}.

Keywords Zeolite, Biochar, Slow-release fertilizers, Green synthesis, Iron nanoparticles, Sustainable agriculture

†Mengqiao Wu and Zefeng Ruan contributed equally to this work.

*Correspondence:
Chengfang Song
songcf@zafu.edu.cn
Bing Yu
bing.yu@zafu.edu.cn

Springer

Graphical Abstract

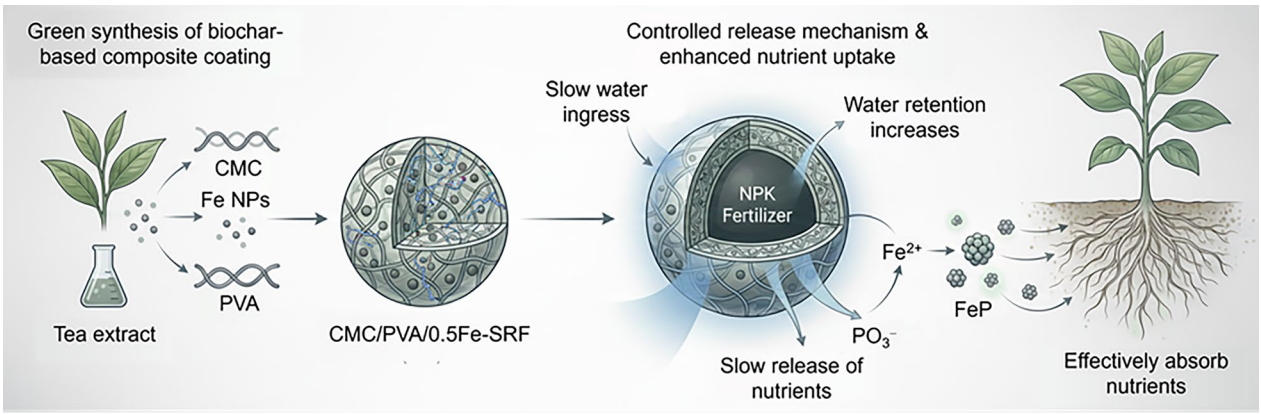

1 Introduction

The escalating global population and intensifying climate change have placed unprecedented demands on agricultural productivity, necessitating innovative strategies to enhance nutrient use efficiency while mitigating environmental degradation (Xu et al. 2025). Conventional fertilizers, though pivotal in sustaining crop yields, suffer from rapid nutrient leaching and volatilization, resulting in substantial economic losses and ecological repercussions such as eutrophication, groundwater contamination, and greenhouse gas emissions (Lu et al. 2023). To address these challenges, slow-release fertilizers (SRFs) have emerged as a transformative solution, designed to synchronize nutrient release with plant uptake dynamics (Nayak et al. 2024). However, the efficacy of SRFs critically hinges on the development of advanced coating materials that balance controlled nutrient diffusion, mechanical robustness, biodegradability, and environmental compatibility (Cheng et al. 2024).

Biochar, a carbonaceous matrix derived from pyrolyzed biomass, has garnered significant attention as a sustainable carrier for SRFs due to its hierarchical porosity, high surface area, and innate nutrient retention capacity (Wang et al. 2024). Its inherent ability to improve soil structure, enhance microbial activity, and sequester carbon further underscores its agronomic and environmental appeal (Gao et al. 2022; Zhou et al. 2025a; Zhou et al. 2026). Nevertheless, unmodified biochar-based SRFs often exhibit suboptimal nutrient release profiles, characterized by premature burst release or incomplete liberation, necessitating the integration of functional coatings to modulate diffusion kinetics (Yang et al. 2025). While synthetic polymer coatings (e.g., polyurethane, polyethylene) offer precise release control, their non-biodegradability and persistence in ecosystems pose long-term ecological risks (Tang et al. 2025). Conversely, biopolymer-based coatings such as carboxymethyl cellulose (CMC) blended with polyvinyl alcohol (PVA)—a water-soluble, renewable binary system with enhanced film-forming ability and mechanical stability—present a greener alternative but are limited by inherent weaknesses in mechanical strength, hydrophilicity, and susceptibility to microbial degradation (Dong et al. 2023; Kassem et al. 2022).

Recent advances in nanotechnology have unveiled the potential of nanoscale reinforcements to augment the performance of biopolymer matrices (Li et al. 2025). In particular, iron-based nanoparticles (Fe-NPs) have shown promise in fortifying the mechanical integrity of composite materials and improving nutrient retention (Lu et al. 2025). However, conventional Fe-NP synthesis routes often involve toxic reductants or stabilizers, contradicting the principles of green chemistry (Xu et al. 2024). The green synthesis of nano-scale iron materials, especially from plants, has garnered substantial attention due to its ease of application, eco-friendly nature, and low cost (Öğütveren and Öğütveren 2017). The integration of phytogenic or microbially mediated green synthesis approaches—utilizing plant extracts or microbial metabolites as reducing and capping agents—offers a sustainable pathway to fabricate eco-friendly Fe-NPs with tailored physicochemical properties (Xiao et al. 2025). In a related approach, nano zero-valent iron supported on Chinese medicine residue-derived carbon was fabricated via a green tea extract reduction method, which proved to be an effective and reusable material for the concurrent removal of Cr(VI) and Cd(II) from aqueous solutions (Diao et al. 2023). Notably, the strategic incorporation of

such nanoparticles into CMC/PVA matrices could synergistically address the limitations of zeolite–biochar hybrid SRFs by (1) fortifying the coating's structural integrity and hydrophobicity and (2) supplying bioavailable iron as a micronutrient to combat widespread iron deficiency in calcareous soils (Tyagi and Thakur 2023). Despite these prospects, the design of green-synthesized nano-iron reinforced CMC coatings for biochar-based SRFs remains unexplored, with critical knowledge gaps persisting in nutrient release mechanisms and agronomic performance.

To overcome the inherent weaknesses of the pristine CMC/PVA coating such as its excessive hydrophilicity and moderate mechanical strength and to construct a highly efficient slow-release system, we engineered a hierarchical fertilizer with a synergistic core–shell architecture. The design is premised on a functional composite core, where a zeolite–biochar hybrid matrix serves as a porous, adsorptive nutrient reservoir for hosting the NPK granules. In this configuration, biochar (with its high surface area and oxygenous groups) synergizes with zeolite (with its ordered porosity and high cation exchange capacity) to form a complementary structure for retaining NH_4^+ and PO_4^{3-}, respectively. This core is then encapsulated by a primary barrier of crosslinked CMC/PVA membrane to control water ingress and initial nutrient diffusion. Crucially, we introduce an innovative secondary reinforcement: green-synthesized tea extract iron nanoparticles (T-FeNPs) are incorporated into the CMC/PVA matrix. The T-FeNPs are expected to densify the coating microstructure and provide active sites for nutrient binding, thereby augmenting the barrier function and introducing iron as a beneficial micronutrient. Consequently, this work aims to: (1) synthesize and characterize the T-FeNPs and their nanocomposite coatings; (2) evaluate the N and P slow-release performance through soil leaching experiments; (3) investigate the agronomic effects on tomato growth and nutrient uptake; and (4) analyze the impact on soil properties and assess the economic and environmental potential of this technology.

2 Materials and methods

2.1 Chemicals

Sodium carboxymethyl cellulose was obtained from Macklin Chemical Technology Co., Ltd. Glycerol ($C_3H_8O_3$) and ferrous sulfate heptahydrate ($FeSO_4{\cdot}7H_2O$) were purchased from Sinopharm Chemical Reagent Co. PVA was purchased from Shanghai Yuanye Bio-Technology Co., Ltd., China. Chemical compound fertilizers used in this work were purchased from Sichuan Greenhope Co., Ltd., China. The natural zeolite powder (1250 mesh) was purchased from Weifang Damei Bentonite Co., Ltd. RSBC was purchased from Henan Lize Co., Ltd., China. The green tea was obtained from the local farmers in lin'an, Hangzhou, China. The vermiculite used in the experiments was sourced from the Long Garden brand, with a pH value (water extraction) of approximately 6.53. Soil separation analysis revealed a composition of 32.33% gravel, 64.22% sand, and 2.57% clay. All the suspensions and solutions in this experiment were made using deionized water.

2.2 Green synthesis of iron nanoparticles

Green tea was subjected to thorough washing with deionized water to remove any surface dust particles, followed by air-drying at room temperature. A total of 15 g of tea leaves was then immersed in 250 mL of deionized water and boiled for 1 h. The resulting extract was subsequently vacuum filtered and stored at 4 °C for future use (Wang et al. 2014).

The extract was mixed with 0.10 M $FeSO_4{\cdot}7H_2O$ in a volume ratio of 2:1 and stirred continuously at room temperature for 30 min. This process led to the synthesis of T-FeNPs. The immediate formation of a black color indicated the reduction of Fe^{2+} ions (Devatha et al. 2016). Subsequently, the synthesized iron nanoparticles were collected through vacuum filtration and washed three times with ethanol. The nanoparticles were then vacuum dried at 50 °C for 12 h and stored in a nitrogen atmosphere for preservation (Kumar et al. 2021, 2023). The yield of the synthesized T-FeNPs, calculated as the mass of dried product relative to the mass of iron in the $FeSO_4{\cdot}7H_2O$ precursor, was approximately 65%.

2.3 Preparation of slow-release fertilizers

The zeolite, composite NPK fertilizer, and RSBC were mixed homogeneously in a mass ratio of 15:65:20 and subsequently subjected to crushing using a pulverizer (Fig. 1). The zeolite and RSBC used were both passed through a 100-mesh sieve, with specific surface areas of 54.47 $m^2\ g^{-1}$ and 19.60 $m^2\ g^{-1}$, respectively, and average pore diameters of 6.11 nm and 10.43 nm. The RSBC contains 68.39 wt % carbon (C), 1.14 wt % nitrogen (N), and 30.48 wt % oxygen (O). The crushed mixture was then placed into a disc granulator set at a 45° inclination angle and rotated at 20 rpm to facilitate the formation of granules. After granulation, the resulting granular fertilizer was screened through a mesh with apertures ranging from 2 to 4 mm. The screened granules were then dried in an oven at 40 °C for 1 h to yield a dried fertilizer core. The core of the fertilizer involves thoroughly mixing the composite fertilizer with zeolite and RSBC, using zeolite and RSBC as nutrient reservoir for the composite fertilizer to retain and slow down the release of nutrients.

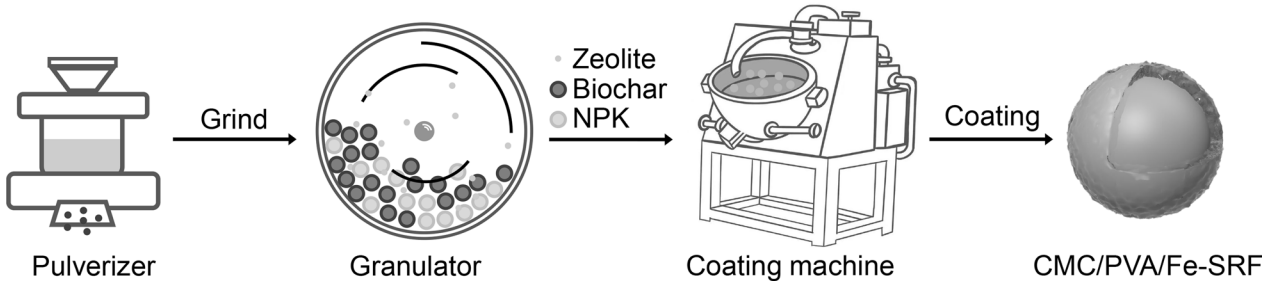

Fig. 1 Schematic of synthesis process of CMC/PVA/Fe-SRF

A total of 3 g of PVA was dissolved in 150 mL of deionized water by stirring at 90 °C using a thermostatic magnetic stirrer until complete dissolution was achieved. After the PVA solution was cooled to 50 °C, the required amounts of T-FeNPs (0 g, 0.15 g, 0.3 g, and 0.5 g) were introduced and stirred to ensure thorough dispersion. The coating liquid was prepared by adding 3 g of CMC and maintaining a constant temperature of 50 °C for 2 h to ensure complete dissolution of the CMC (Channab et al. 2024). The slow-release fertilizer composite was synthesized by spraying the coating liquid onto the surface of the dried fertilizer core, followed by drying using a coating machine to facilitate the formation of a uniform coating. The resulting fertilizers were designated as CMC/PVA-SRF, CMC/PVA/0.15Fe-SRF, CMC/PVA/0.3Fe-SRF, and CMC/PVA/0.5Fe-SRF, respectively.

2.4 Characterization

The morphologies of the prepared hydrogel films were characterized using a scanning electron microscope (SEM, Hitachi, Japan) at a working voltage of 3.00 kV. The hydrogel films were affixed to copper sheets using conductive adhesive and then coated with a gold layer. The crystal structure of the prepared T-FeNPs was analyzed with an X-ray diffractometer (XRD, Rigaku Ultima IV, Japan) at a scan rate of 2° min^{-1}. The surface composition of the T-FeNPs was examined using X-ray photoelectron spectroscopy (XPS, Thermo Fisher Scientific, UK) with monochromatic Al Kα radiation (1486.6 eV, 6 mA filament current).

2.5 Slow-release performance of various fertilizers

The soil column leaching test was used to investigate the slow-release characteristics of formulated fertilizers. Briefly, 100 g of vermiculite with a moisture content of 60% was placed in each column. A 0.1 g sample of each fertilizer was placed 5 cm beneath the surface of the vermiculite (Wu et al. 2025). Each fertilizer formulation (including controls) was tested in triplicate using independent soil columns (n = 3). Forty milliliters of deionized water was applied uniformly to the soil columns at fixed intervals, and the leachate collected from the bottom was analyzed for nitrogen (N) and phosphorus (P) release. The release kinetics of the fertilizers were analyzed using the following kinetic models:

$$\text{Zero-order kinetics}: q = ax + b \tag{1}$$

$$\text{First-order kinetics}: q = a(1 - e^{-k_1 t}) \tag{2}$$

$$\text{Ritger-Peppas model}: q = k_R t^n \tag{3}$$

$$\text{Higuchi model}: q = at^{1/2} + b \tag{4}$$

where q is the release ratio of N and P at different time intervals, and k_1, k_R, and n are the release rate constants.

2.6 Water-retention capacities of various fertilizers

First, 0.1 g of fertilizer was mixed with 40 g of vermiculite in a cup to study the water retention capacity of different fertilizers. Then, 50 mL of deionized water was added to the cup and the initial total weight was recorded as W_0. All the experiments were carried out at room temperature and the weight of the cup was measured at regular intervals (W_T). The soil water retention ratio (W_R%) was calculated as follows (Lu et al. 2025):

$$WW_R\% = (W_0 \times W_T)/W_0 \times 100\% \tag{5}$$

where W_0 is the mass of soil and fertilizer in general on the first day, W_T is the overall mass of soil and fertilizer on day T, and W_R% is soil water-retention ratio.

2.7 Pot experiment

Tomato seedlings of similar size were transplanted into pots containing a mixture of vermiculite and peat soil, and maintained under natural light conditions at 25 °C to 30 °C. The potting experiment utilized a standardized and reproducible substrate, consisting of a homogeneous mixture of vermiculite and peat soil in a volume ratio

of 2:3. This mixture provides a consistent, low-nutrient background growth environment with good aeration and water retention capacity, making it ideal for assessing fertilizer effects without significant interference from variations in the native soil. The physicochemical properties of this formulated potting mixture are presented in Table S1. Fertilization was applied twice, on the 1st and 30th days after transplantation, with 1 g of fertilizer per application (Cheng et al. 2024). The control group consisted of plants without fertilization (CK) and those receiving a compound NPK fertilizers (NPK). The plants were grown for 60 days, with regular measurements of plant height. Each treatment was applied to three independent tomato plants (n = 3), arranged in a completely randomized design. After harvest, the plants were rinsed with deionized water, blotted dry on absorbent paper, and then assessed for fresh weight and root length. The plants were oven-dried at 105 °C for 30 min, followed by drying at 70 °C until completely dry, and dry weight was recorded (Dong et al. 2025). Finally, the total nitrogen and total phosphorus content of the plants were quantitatively measured, with each measurement repeated three times.

2.8 Calculation of greenhouse gas emissions

The greenhouse gas emissions (GHG) resulting from the nitrogen component in NPK compound fertilizer during its application phase can be calculated using the following Eqs. (6)–(9).

$$E_{directN_2O} = W_N \times EF_1 \times \frac{44}{28} \times 273 \quad (6)$$

$$E_{GASF} = W_N \times Frac_{GASF} \times EF_4 \times \frac{44}{28} \times 273 \quad (7)$$

$$E_{LEACH} = W_N \times Frac_{LEACH} \times EF_5 \times \frac{44}{28} \times 273 \quad (8)$$

$$E_{limestone} = W_N \times LT \times 0.12 \times 44 \quad (9)$$

where W_N is the amount of an applied nitrogen from NPK compound (Mt N); $\frac{44}{28}$ is the ratio used to convert the mass of N_2O–N to N_2O (Buendia et al. 2019; Gao and Cabrera Serrenho 2023); and 273 is the 100-year global warming potential of N_2O, as updated by the IPCC AR6 WGI. In Eq. (7), $Frac_{GASF}$ (Buendia et al. 2019) represents the fraction of nitrogen in the NPK compound that volatilizes as ammonia (NH_3) and nitrogen oxides (NO_x). In Eq. (8), $Frac_{LEACH}$ represents the fraction of nitrogen in the NPK compound that leaches as nitrate (NO_3^-), and EF_4 and EF_5 represent the emission factors for N_2O resulting from atmospheric deposition of nitrogen and the N_2O emission from leached nitrate, respectively. These values are based on the IPCC 2019 refinement to the 2006 IPCC greenhouse gas inventories (Buendia et al. 2019). In Eq. (9), LT is the amount of limestone required to neutralize the soil per ton of applied nitrogen, 0.12 represents the fraction of carbon element in calcium carbonate ($CaCO_3$), and $\frac{44}{12}$ is to convert the relative molecule weight of carbon (C) to CO_2.

2.9 Statistical analysis

The data were analyzed using a one-way analysis of variance (ANOVA) performed with SPSS software (version 27.0, SPSS Inc.). The experiment was conducted in triplicate, and the mean values were reported. Statistically significant differences ($p < 0.05$) are indicated by different letters in all tables and figures.

3 Results and discussion

3.1 Synthesis and characterization of CMC/PVA/Fe NPs

Iron nanoparticles (T-FeNPs) were successfully green-synthesized using tea extract and incorporated into CMC/PVA matrices. The rapid bioreduction of Fe^{2+} was visually confirmed by the immediate formation of a black suspension (Fig. 2a, b).

SEM analysis revealed that the synthesized T-FeNPs were predominantly spherical with a relatively uniform size distribution averaging approximately 50–100 nm (Fig. 2c). Some degree of aggregation was observed, which is typical for biogenically synthesized nanoparticles due to the presence of organic capping agents from the tea extract. XRD analysis (Fig. 2d) indicated that the T-FeNPs possessed a largely amorphous or poorly crystalline structure. The broad hump centered around 20–35° (2θ) is characteristic of iron oxide/hydroxide phases (e.g., magnetite (Fe_3O_4), maghemite (γ-Fe_2O_3), or ferrihydrite) commonly formed under green synthesis conditions, consistent with the observed black color (Wang et al. 2013; Wu et al. 2019). The absence of sharp, distinct peaks further supports the dominance of nanoscale or amorphous iron (oxyhydr) oxide phases (Wang et al. 2014).

XPS analysis of the Fe 2*p* region (Fig. 2e) provided insight into the surface chemistry and oxidation states of the T-FeNPs. The spectrum exhibited characteristic peaks for Fe^{3+}, with Fe $2p_{3/2}$ and Fe $2p_{1/2}$ binding energies observed near 711.0 eV and 724.5 eV (Qu et al. 2019; Xiang et al. 2022), respectively, accompanied by distinct satellite peaks around 719 eV (Li and Zhao 2017). A minor contribution from Fe^{2+} (Fe $2p_{3/2}$ ~ 709.5 eV) was also detectable, suggesting the potential presence of a mixed-valence iron oxide phase (e.g., magnetite, Fe_3O_4) or partial surface oxidation. This confirms the successful

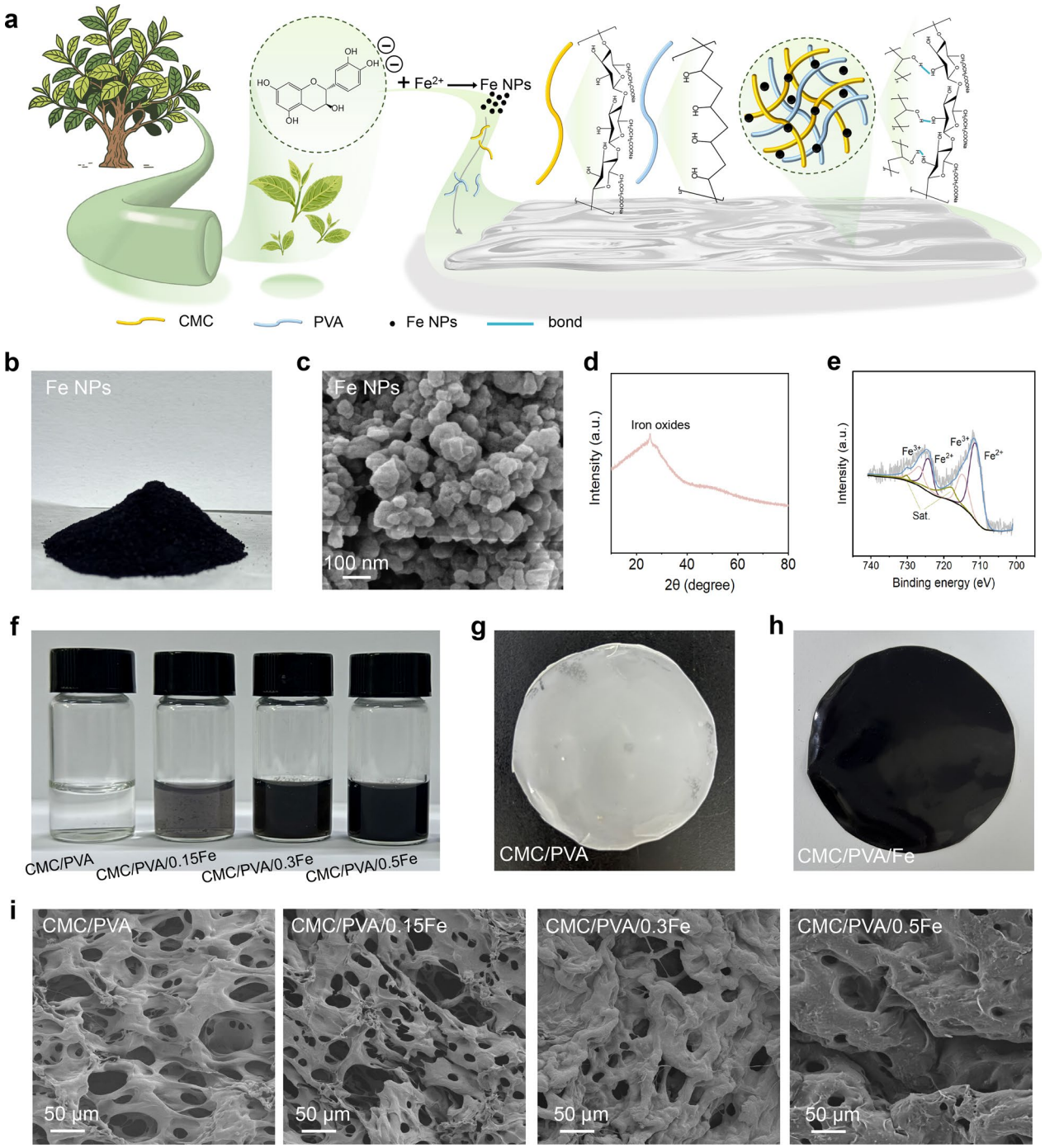

Fig. 2 **a** Synthesis schematic of the CMC/PVA/Fe coating. **b** Digital image and **c** SEM micrograph (scale bar: ~ 100 nm) of the as-prepared spherical T-FeNPs. **d**, **e** Material characterization by XRD and Fe 2p XPS. **f** CMC/PVA/Fe precursor solution. **g**–**i** Film formation: photographs of pure **g** and composite **h** films, and **i** cross-sectional SEM images showing the effect of increasing Fe content (0 to 0.5 wt%).

conversion of Fe^{2+} ions primarily to Fe^{3+} species, stabilized by the phytochemical capping agents.

The CMC/PVA coating solution containing dispersed T-FeNPs exhibited a homogeneous dark brown/black appearance (Fig. 2f), contrasting with the translucent appearance of the pure CMC/PVA solution, visually confirming the integration of the nanoparticles. Cast films of the nanocomposite (CMC/PVA/Fe) were successfully

formed (Fig. 2g, h). SEM analysis of CMC/PVA/Fe film cross-sections (Fig. 2i) showed that increasing T-FeNPs loading progressively densified the matrix. The pure CMC/PVA film exhibited an open, porous structure, while embedded nanoparticles at lower loadings (0.15Fe, 0.3Fe) reduced pore size. At the highest loading (0.5Fe), significant nanoparticle aggregation resulted in a markedly denser, less porous microstructure, where pores were largely filled by T-FeNPs. This reduction in pore size and connectivity creates more tortuous diffusion pathways, enhancing the coating's barrier function for sustained nutrient release.

The analysis of the scanning electron microscope (SEM) images of the fertilizer cross-section (Fig. S1a) indicated that a consistent and substantial physical barrier had formed on the surface of the CMC/PVA/0.5Fe-SRD particles, with a thickness of approximately 24.02 μm. This barrier serves as the fundamental basis for the controlled release mechanism. The macroscopic physical properties of the coated fertilizers were also consistent (Fig. S1b). The granules of the optimal CMC/PVA/0.5Fe-SRF formulation exhibited a uniform spherical morphology with an average diameter of approximately 6.76 mm, indicating a reproducible coating process suitable for field application. To further evaluate the change in surface properties, static water contact angles were measured on pure CMC/PVA and CMC/PVA/0.5Fe composite films. The results showed a significant increase from 60.1° to 68.9° upon the incorporation of T-FeNPs, providing direct evidence for the enhanced hydrophobicity of the nanocomposite coating, which contributes to retarding water penetration into the fertilizer core (Fig. S1c).

3.2 Slow-release of nutrients of the prepared fertilizers

Soil column leaching experiments (Fig. 3a) were conducted to evaluate the slow-release performance of the fertilizers. Cumulative N and P release over 30 days (Fig. 3b, c) showed two phases: a rapid leaching phase (0–10 days) followed by a sustained slow-release phase (10–30 days). Conventional NPK released most nutrients within 10 days, whereas all coated fertilizers exhibited prolonged release. Notably, T-FeNPs-incorporated fertilizers, especially CMC/PVA/0.5Fe-SRF, showed the slowest initial release and the lowest cumulative nutrient loss, highlighting the key role of T-FeNPs in enhancing the coating's nutrient-retention capacity.

Over the entire 30-day release cycle, the "Without Fe" treatment (CMC/PVA-SRF) reduced cumulative N and

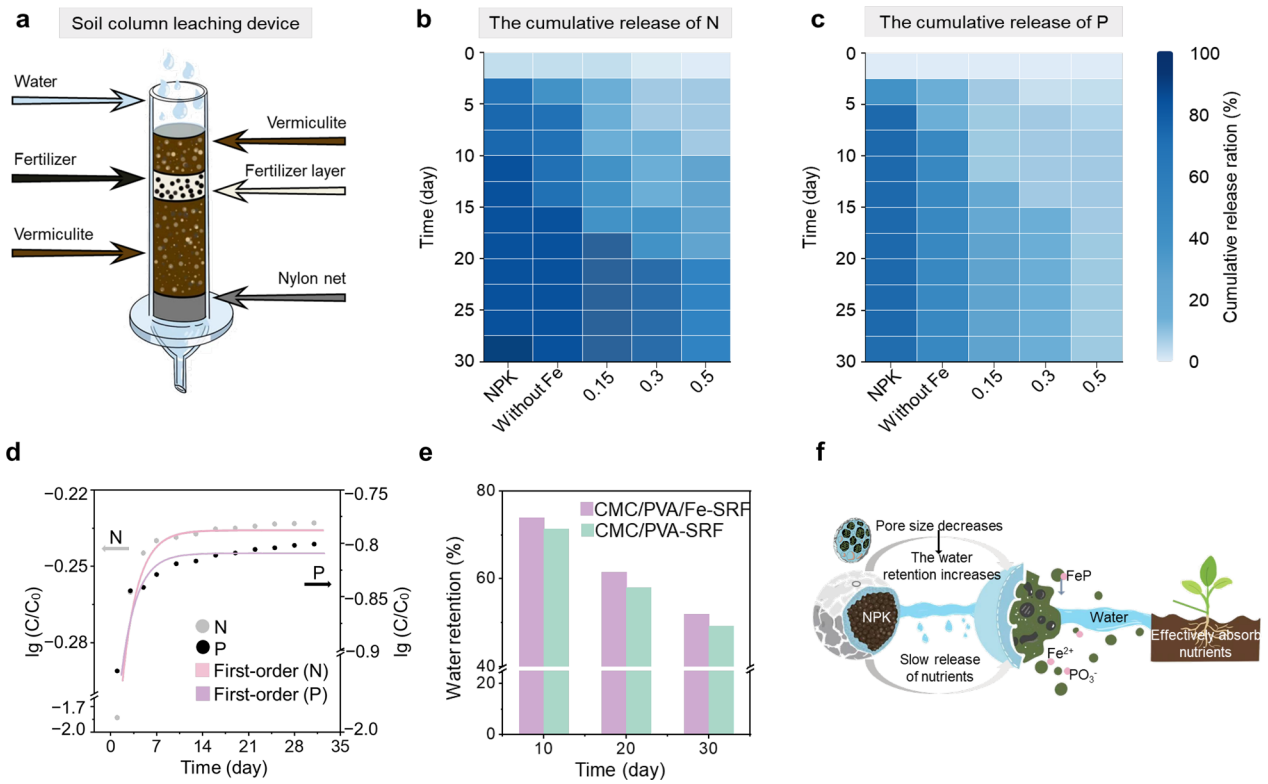

Fig. 3 **a** The schematic diagram of the soil column leaching apparatus. The slow-release of **b** N, and **c** P from various fertilizers in soil. The release kinetics of **d** N, and P from CMC/PVA/0.5Fe-SRF. **e** The water-retention capabilities of soils with the addition of various fertilizers. **f** A schematic illustration of the nutrient release mechanism of CMC/PVA/0.5Fe-SRF.

P release by 2.77% and 27.91%, respectively, compared to conventional NPK. The significantly lower P release rate in the "Without Fe" group relative to NPK indicates heightened sensitivity of P to the presence of the coating barrier. This effect arises from the core structural design of the fertilizer system: a zeolite–biochar composite serves as the NPK nutrient reservoir, encapsulated by an outer CMC-PVA crosslinked membrane acting as a physical barrier. Biochar, with its high specific surface area and abundant oxygen-containing functional groups, synergizes with zeolite characterized by ordered porosity and strong cation exchange capacity to form a functionally complementary dual-porous architecture. Zeolite dominates ion-exchange adsorption of NH_4^+ (Zhan et al. 2023), while biochar immobilizes PO_4^{3-} via electrostatic attraction and ligand exchange (Huang et al. 2020), collectively achieving nutrient retention through synergistic effects.

This intermediate performance confirms that even without nano-reinforcement, the CMC/PVA coating itself provides a significant diffusion barrier compared to uncoated NPK (Channab et al. 2024). The further reduction in nutrient release observed in the T-FeNPs-incorporated groups (CMC/PVA/Fe-SRFs) is attributed to the microstructural modification of the coating. As revealed by SEM (Fig. 2i), the incorporated T-FeNPs interact with the biopolymer matrix, leading to a progressive densification and a reduction in pore size and connectivity as the loading increases. This microstructural evolution creates more tortuous diffusion pathways, imposing greater resistance to the outward migration of dissolved nutrients. Consequently, with increasing T-FeNPs content (from 0.15 to 0.5 g), cumulative N release decreased from 69.61% to 58.47%, and P release declined from 27.01% to 15.82%, demonstrating a clear concentration-dependent enhancement in leaching resistance.

The divergent release kinetics of N and P stem from their distinct interaction mechanisms with the coating/zeolite–biochar matrix. Unmodified zeolite and biochar exhibit limited capacity to immobilize NH_4^+ via ion exchange and electrostatic attraction, consistent with previous studies (Chen et al. 2021; Jha and Hayashi 2009). While the surfaces of T-FeNPs (predominantly iron oxides/hydroxides as per XRD/XPS, Fig. 2d, e) can adsorb cations, this binding is relatively less stable compared to their interaction with phosphate (Liang et al. 2014). For PO_4^{3-}, immobilization is significantly stronger, primarily relying on surface complexation with the iron (oxyhydr) oxide nanoparticles (T-FeNPs) and potential formation of insoluble Fe–P phases (e.g., strengite-like compounds). Higher T-FeNPs content provides more surface sites for phosphate binding, leading to the significantly lower P release observed in the 0.3Fe and 0.5Fe treatments compared to the 0.15Fe group (Sun et al. 2021). Notably, the 0.5Fe group achieved the lowest cumulative P release (15.82%), confirming that P leaching inhibition is markedly enhanced with increasing T-FeNPs concentration. Notably, the long-term efficacy of the T-FeNPs within the coating relies on the stabilizing effect of the CMC-PVA matrix. This polymeric network helps prevent nanoparticle agglomeration and retards water infiltration by forming a physical barrier, thereby sustaining nutrient immobilization. As shown in Fig. 3b, c, the 0.5Fe group maintained the lowest N and P release rates throughout the 30-day period, validating the long-term slow-release effectiveness of the T-FeNPs reinforced CMC-PVA coating. To objectively evaluate the nutrient control efficacy of our optimal CMC/PVA/0.5Fe-SRF formulation, we compared its performance with other slow-release fertilizers in terms of cumulative nitrogen and phosphorus release, as shown in Table S2. Our material exhibits excellent phosphorus retention (15.8% release) and outstanding nitrogen retention (58.5% release), demonstrating a strong competitive edge. This comparison underscores that our green manufacturing strategy does not compromise performance; rather, it provides a favorable nutrient release profile along with inherent sustainability benefits.

The incorporation of well-dispersed T-FeNPs indeed enhances the mechanical robustness of the CMC/PVA coating (Fig. S2). The tensile strength of the CMC/PVA/0.5Fe composite is significantly higher than that of the pure CMC/PVA film, confirming that the nanoparticles have reinforced the polymer film. Although the composite exhibits lower fracture strain (elongation), indicating a trade-off between increased stiffness and reduced ductility, this characteristic transition is highly beneficial for our specific application. As a fertilizer coating, the primary requirements are: (1) sufficient strength and stiffness to withstand mechanical stresses from soil particles during handling and compaction without fracturing; and (2) a dense, intact barrier that controls the release of nutrients over time. Due to its lower toughness and higher rigidity, the coating is less prone to deformation and crack formation under gravitational forces. Therefore, T-FeNPs enhance the functional stability of the coating by improving its mechanical strength and structural integrity. This ensures that the coating maintains physical integrity and functional efficacy throughout the release period, as evidenced by the sustained nutrient release curve over 30 days (Fig. 3b, c).

The release kinetics of N and P in the soil column leaching experiment were systematically analyzed using zero-order, first-order, Ritger–Peppas, and Higuchi models. As shown in Fig. 3d, the release profile of CMC/PVA/0.5Fe-SRF best fitted the first-order kinetic model

($R^2 > 0.89$) (Costa and Lobo 2001), effectively elucidating the sustained-release behavior of the fertilizer resulting from gradual dissolution upon water contact in the soil (Han et al. 2023; Shaghaleh et al. 2022). This indicates that the release process was primarily governed by the concentration gradient. Under this mechanism, the release rate increases when the internal concentration is high and the external concentration is low; conversely, as the external concentration rises (Adepu and Khandelwal 2020), the release rate progressively decreases. This mechanism is typically associated with a diffusion process, where the concentration gradient acts as the driving force for release.

Water retention performance in soil was evaluated for fertilizers containing T-FeNPs versus those without T-FeNPs. As depicted in Fig. 3e, measurements taken at 10, 20, and 30 days revealed that the T-FeNP-containing fertilizer exhibited water retention rates higher by 2.65%, 3.54%, and 2.59%, respectively, compared to the non-FeNP fertilizer at the corresponding time points, maintaining consistently higher moisture levels. The observed enhancement in soil water retention is primarily attributed to the formation of a denser membrane layer and reduced pore size, thereby minimizing water loss.

The core slow-release mechanism of this fertilizer lies in the synergistic interplay between the CMC/PVA/Fe composite coating and the zeolite/biochar core (Fig. 3f). Primarily, the physical barrier mechanism dominates: T-FeNPs clog the pores within the CMC/PVA matrix, significantly reducing the coating's pore size and connectivity. This forms a dense, tortuous diffusion pathway that effectively blocks rapid soil moisture intrusion into the fertilizer core, preventing premature swelling or rupture of the coating and substantially impeding both water penetration and outward migration of dissolved nutrient ions. Fourier Transform Infrared Spectroscopy (FTIR) analysis was performed on the membranes before and after slow release (Fig. S3). The three peaks at 1125, 1051, and 974 cm^{-1} can mainly be attributed to the bending vibrations of hydroxyl groups (Fe–OH) in iron (hydroxide) oxides. After reacting with phosphate, a new bending band appeared at 1018 cm^{-1}, which was assigned to the asymmetric vibration of P–O (Zhang et al. 2009). The surface hydroxyl groups were replaced by phosphates, and the P–O bond changes when coordinating to Fe^{3+} sites, confirming the formation of the Fe–O–P bond. This indicates that T-FeNPs provide active surface sites to fix PO_4^{3-} through strong surface complexation, thereby inhibiting the release of phosphorus. Furthermore, the dense coating enhances the water retention capacity of the local soil and optimizes moisture control. This synergistic mechanism collectively transforms nutrient release from a rapid leaching process into a slow, concentration-gradient-driven transmembrane diffusion process.

3.3 Agronomic performance of the coated fertilizers in tomato cultivation

The pot experiment unequivocally demonstrated the superiority of T-FeNPs-reinforced coatings in enhancing tomato growth and nutrient efficiency. Plants treated with CMC/PVA/0.50Fe-SRF achieved the greatest height (46 cm), significantly outperforming other coated variants (23–40.6 cm), NPK (31.2 cm), and the control (CK, 17 cm) at harvest (Fig. 4a). This growth advantage emerged early (Day 30: ~17 cm vs. NPK/CK at ~14 cm), underscoring the role of sustained nutrient release in avoiding initial growth stagnation common with conventional fertilizers (Chen et al. 2023).

Root elongation exhibited a nanoparticle concentration-dependent response (Fig. 4b). The longest roots (~29 cm) occurred in CMC/PVA/0.50Fe-SRF and 0.30Fe-SRF treatments, contrasting sharply with NPK-induced salt-avoidance elongation, a stress response to rapid nutrient surge (Goldsmith et al. 2020). This divergence highlights how gradual nutrient release from FeNPs-composites promoted deeper root exploration for water/nutrients, while NPK's burst release confined roots to surface layers (Shahzad et al. 2025). Notably, intermediate Fe-loading (0.15Fe-SRF) and unmodified CMC/PVA-SRF yielded shorter but potentially denser roots, suggesting a trade-off between root extension and branching under moderated nutrient flux.

Biomass data further validated coating efficacy (Fig. 4c, d). CMC/PVA/0.50Fe-SRF maximized fresh (20.77 g) and dry weight (2.88 g), exceeding NPK (FW: 17.6 g; DW: 2.03 g) by 18% and 42%, respectively. The DW/FW ratio was highest in 0.50Fe-SRF (13.9%), indicating superior photosynthetic efficiency and carbon partitioning, likely due to: (1) Iron nutrition: T-FeNPs supplied bioavailable Fe, mitigating chlorosis (Therby-Vale et al. 2022) and enhancing redox metabolism (e.g., photosystem I efficiency); (2) Water-nutrient synergy: Improved soil moisture retention (Fig. 3e) reduced drought stress, sustaining turgor-driven cell expansion.

Nutrient uptake patterns (Fig. 4e, f) revealed complex interactions between the coating formulations and plant assimilation. Conventional NPK fertilizer resulted in the highest total nitrogen content in plant tissue (14.5 g kg^{-1}), attributable to its rapid initial nutrient release. Among the coated fertilizers, CMC/PVA/0.50Fe-SRF achieved comparable nitrogen uptake (13.2 g kg^{-1}), while CMC/PVA/0.30Fe-SRF showed the lowest nitrogen content (10.36 g kg^{-1}). Phosphorus uptake exhibited a different pattern, with CMC/PVA/0.30Fe-SRF achieving the highest phosphorus content (1.44 g kg^{-1}), exceeding

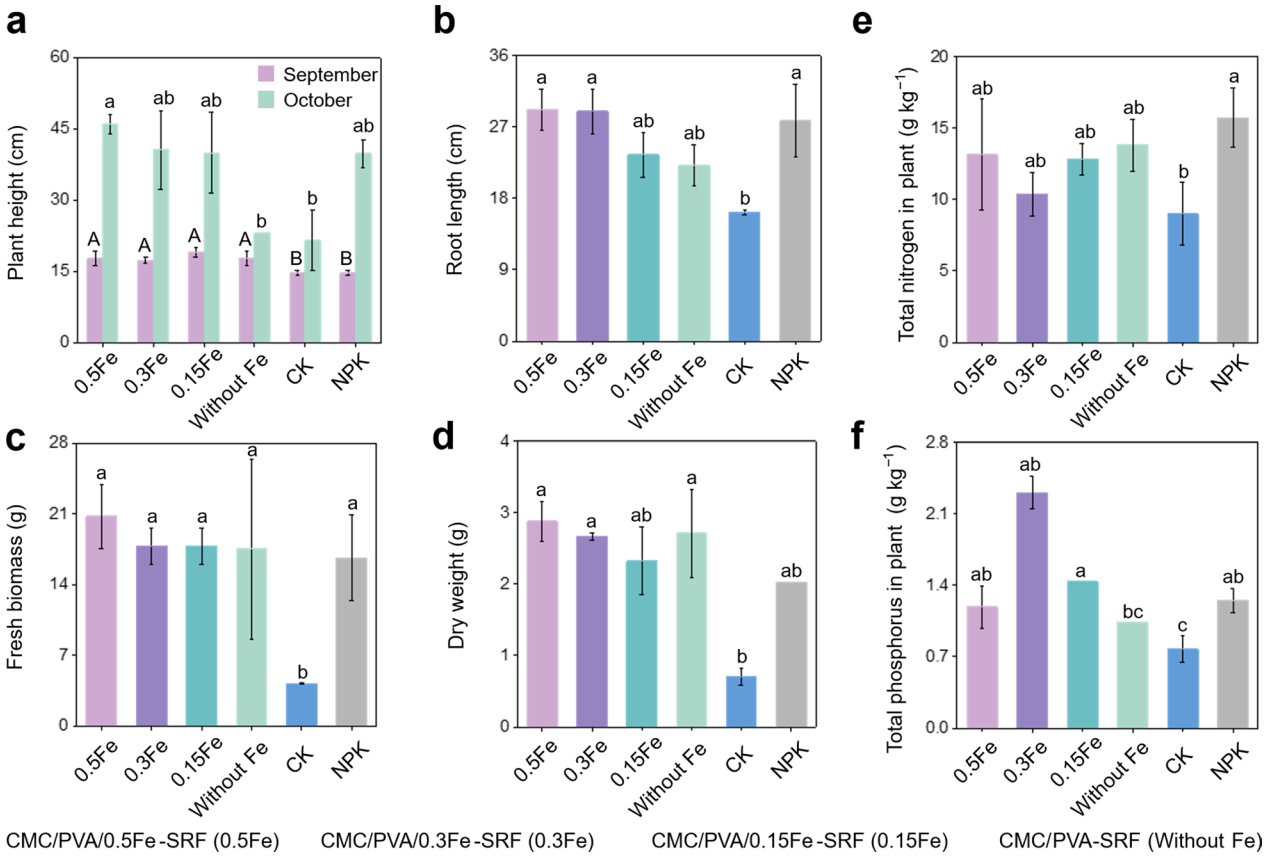

Fig. 4 **a** Plant height of tomato at 30 and 60 days after planting under different fertilizer treatments. **b** Root length of tomato plants at harvest (60 days). **c** Fresh weight and **d** dry weight of tomato plants at harvest (60 days). **e** Total nitrogen and **f** total phosphorus uptake in tomato plants at harvest (60 days). Different letters indicate significant differences among treatments at $p < 0.05$

both conventional NPK (1.25 g kg^{-1}) and the high-loading CMC/PVA/0.50Fe-SRF treatment (1.15 g kg^{-1}). This suggests an optimal intermediate FeNPs concentration for phosphorus availability, potentially balancing between phosphorus retention by iron phases and phosphorus solubilization. The superior growth performance of CMC/PVA/0.50Fe-SRF despite its moderate phosphorus uptake highlights the contribution of the iron nanoparticles themselves as a micronutrient source, particularly beneficial in iron-deficient soils, while simultaneously enhancing the physical barrier function of the coating as demonstrated in leaching tests and SEM characterization.

3.4 Soil physicochemical properties after the application of coated fertilizers

Post-harvest soil analysis was conducted on triplicate soil samples (n = 3) collected from each treatment pot. Post-harvest analysis revealed that T-FeNPs-reinforced coatings significantly enhanced soil nutrient retention and modified key physicochemical properties (Fig. 5). For nitrogen dynamics, total soil N content was highest in T-FeNPs-amended treatments, reaching 58.47 g kg^{-1} (CMC/PVA/0.30Fe-SRF) and 56.31 g kg^{-1} (CMC/PVA/0.50Fe-SRF), compared to 48.33 g kg^{-1} (CMC/PVA-SRF without Fe) and 47.67 g kg^{-1} (NPK). This enhancement may stem from two synergistic mechanisms: (1) the densified coating microstructure reduced pore connectivity, limiting water infiltration and N leaching; and (2) Fe^{3+}-rich T-FeNPs adsorbed NH_4^+ (Dong et al. 2021) via electrostatic interactions while suppressing microbial nitrification through redox activity (Otero et al. 2016). In contrast, available N peaked in conventional NPK (261.08 mg kg^{-1}) and unmodified CMC/PVA-SRF (236.10 mg kg^{-1}), reflecting rapid nutrient release. The inverse relationship between total and available N in T-FeNPs treatments (e.g., 212.45 mg kg^{-1} available N in 0.5Fe-SRF) confirmed their sustained-release functionality.

Phosphorus retention was dramatically improved by T-FeNPs, with total P rising to 1.67 g kg^{-1} in CMC/PVA/0.50Fe-SRF versus 0.91 g kg^{-1} in NPK (Fig. 5b). This resulted from strong chemisorption of PO_4^{3-} onto iron (oxyhydr) oxide surfaces (He et al. 2016). Available P

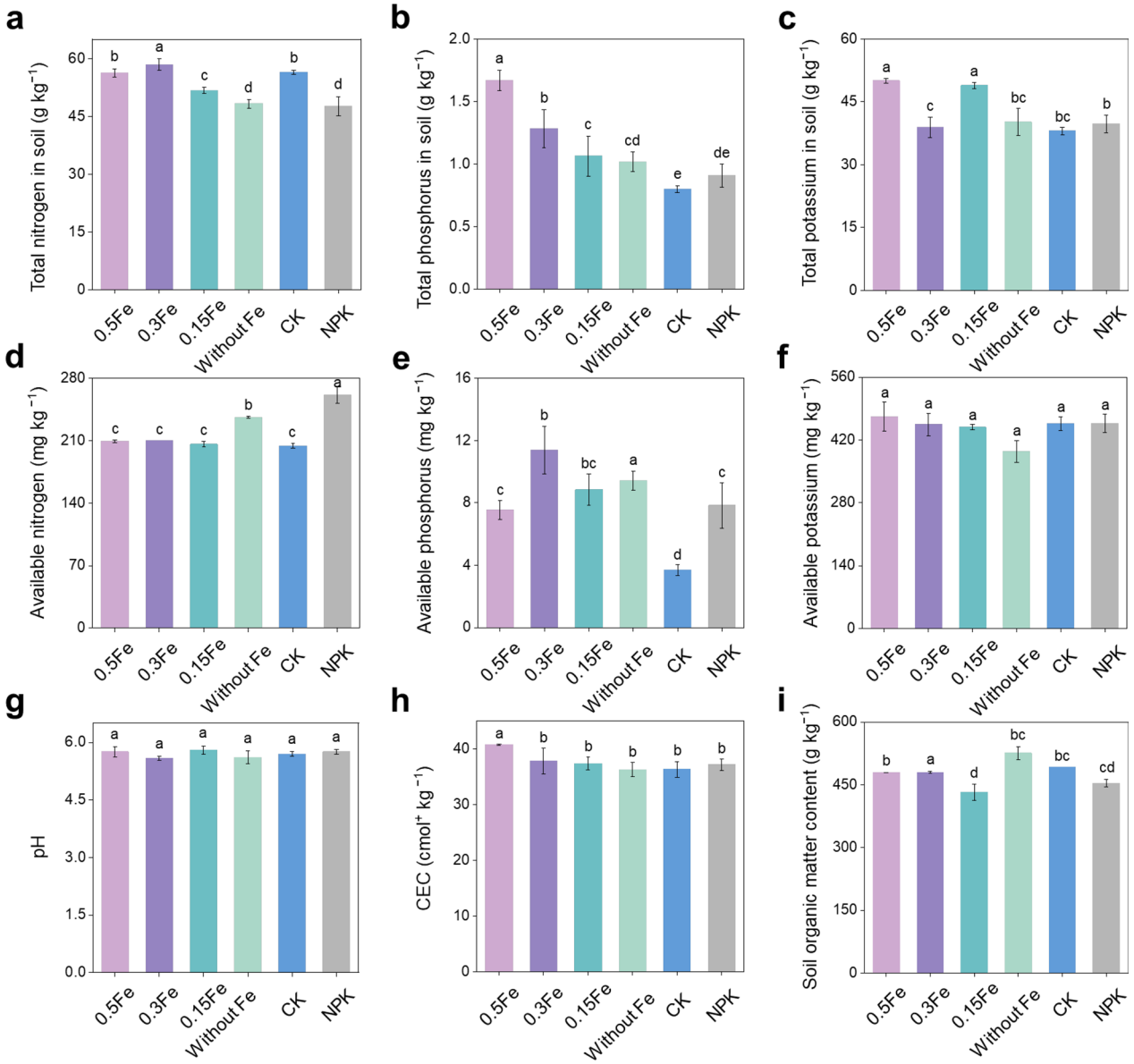

Fig. 5 **a** Total nitrogen in soil. **b** Total phosphorus in soil. **c** Total potassium in soil. **d** Available nitrogen in soil. **e** Available phosphorus in soil. **f** Available potassium in soil. **g** pH of soil. **h** CEC of soil. **i** Soil organic matter content. Different letters indicate significant differences among treatments at $p < 0.05$

exhibited a non-linear response, peaking at 11.38 mg kg^{-1} in the CMC/PVA/0.50Fe-SRF treatment (Fig. 5e), where moderate nanoparticle loading competed with natural soil minerals for phosphate binding, reducing fixation. Higher T-FeNPs loading (CMC/PVA/0.50Fe-SRF) further increased retention but reduced bioavailability (9.85 mg kg^{-1} available P), highlighting a trade-off between storage capacity and release efficiency.

For potassium, total K content increased with T-FeNPs loading (50 g kg^{-1} in CMC/PVA/0.50Fe-SRF vs. 39.7 g kg^{-1} in NPK; Fig. 5c), attributed to complementary retention mechanisms: zeolite's ion-exchange capacity immobilized in the fertilizer core, while T-FeNPs reduced coating permeability to limit leaching. Available K peaked at 454.76 mg kg^{-1} in CMC/PVA/0.30Fe-SRF (Fig. 5f), indicating balanced release kinetics. The slight over-retention in CMC/PVA/0.50Fe-SRF (472.14 mg kg^{-1}) aligned with excessive coating densification observed via SEM.

Soil health indicators exhibited T-FeNPs-mediated optimization. Soil pH remained stable (5.59–5.80; Fig. 5g) due to counteracting effects: OH^- release during iron oxidation neutralized acidity from NPK nitrification. Cation exchange capacity (CEC) increased to 40.73 $cmol^+ kg^{-1}$ in CMC/PVA/0.50Fe-SRF (Fig. 5h), driven by additional charge sites from T-FeNPs-derived iron oxides and carboxyl groups of partially degraded CMC/PVA. Organic matter (OM) content was highest in unmodified CMC/PVA-SRF (525.75 g kg^{-1}) and CMC/PVA/0.30Fe-SRF (479.97 g kg^{-1}; Fig. 5i), suggesting that optimal T-FeNPs loading (0.3%) facilitated controlled coating biodegradation, releasing organic fragments. Higher nanoparticle concentrations (CMC/PVA/0.50Fe-SRF) over-stabilized the matrix, delaying OM release.

3.5 Economic viability and GHG reduction potential

Here, we estimated the cost-effectiveness of CMC/PVA/0.5Fe-SRF based on the current industrial condition. The production cost of CMC/PVA/0.5Fe-SRF was primarily composed of three components: manufacturing, green synthesis, and other expenses. Figure 6a illustrates the proportions and costs of each component in the total fertilizer production cost. The raw materials needed for the green synthesis process, along with the corresponding steps, are thoroughly detailed in Sect. 2.2. Similarly, the necessary raw materials and procedures for manufacturing are outlined in this Sect. 2.1 and 2.2. Other expenses included electricity and maintenance costs. Additionally, the equipment maintenance cost was divided into two components: depreciation and repair. Considering a 10-year depreciation period for the equipment and a 5% residual value, the depreciation expense was calculated based on the CMC/PVA/0.5Fe-SRF workload. Assuming that the equipment had a capacity to process 10,000 tons of CMC/PVA/0.5Fe-SRF over ten years and a total value of US$55,953.55, the depreciation cost per ton of CMC/PVA/0.5Fe-SRF produced was US$5.32. The annual maintenance cost factor for the equipment was 4.5%, totaling US$2,517.91, or US$2.52 t^{-1} of CMC/PVA/0.5Fe-SRF. The estimated electricity cost during the production process ranged from 9.75 to 12.53 cents kWh^{-1}. Each ton of fertilizer required 228.1 kWh, resulting in an electricity cost of US$22.24–28.59 t^{-1} CMC/PVA/0.5Fe-SRF. The CMC/PVA/0.5Fe-SRF production process employed eight workers at an annual cost of US$8,356.55 each person, yielding a total labor cost of US$66,852.37, which contributed US$66.85 to the production cost per ton of CMC/PVA/0.5Fe-SRF. Therefore, the remaining expenses totaled US$100.10 t^{-1} of CMC/

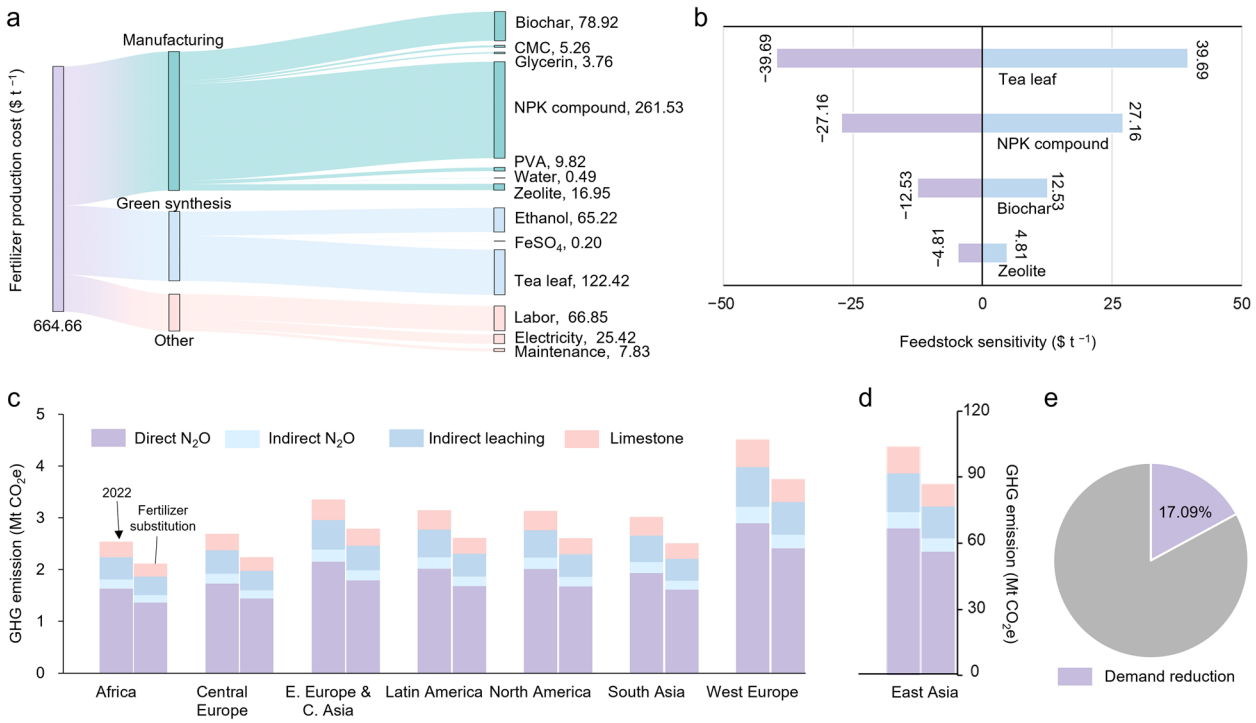

Fig. 6 **a** Sankey diagram illustrating the production cost distribution of a new compound fertilizer. **b** Price sensitivity of feedstock for the new compound fertilizer. **c** Breakdown of GHG from nitrogen in compound fertilizers across seven regions in 2022. Breakdown of these emissions for the East Asia region in 2022 is in **d**. **e** Reduction in nitrogen demand from NPK compounds under the fertilizer substitution scenario.

PVA/0.5Fe-SRF, representing 15.06% of the total fertilizer production cost.

The green synthesis and manufacturing accounted for US$187.84 (28.26%) and US$376.73 (56.68%), respectively, of the production cost per ton of CMC/PVA/0.5Fe-SRF. In the green synthesis process, it was estimated that the production of one ton of CMC/PVA/0.5Fe-SRF required 30 kg of tea leaf, 78.9 kg of ethanol, and 3.8 kg of $FeSO_4$, which contributed US$122.42, US$65.22, and US$0.2, respectively, to the total production cost of the CMC/PVA/0.5Fe-SRF. Furthermore, for the manufacturing components, it was estimated that producing one ton of CMC/PVA/0.5Fe-SRF required 722 kg of NPK compound fertilizer, 222 kg of biochar, 167 kg of zeolite, 6 kg of CMC, 6 kg of PVA, 6 L of glycerol, and 1.16 tons of water. These raw materials contributed US$261.53, US$78.92, US$16.95, US$5.26, US$9.82, US$3.76, and US$0.49, respectively, to the total production cost of the fertilizer. Through the analysis of the current process, the total cost of CMC/PVA/0.5Fe-SRF production for these three parts amounted to US$664.66 t^{-1}.

It was found that the feedstock contributed 84.94% to the production cost of CMC/PVA/0.5Fe-SRF. Therefore, a sensitivity analysis of the feedstock prices for CMC/PVA/0.5Fe-SRF production costs should be conducted. As shown in Fig. 6b, the four feedstocks that had the greatest effect on the production cost of CMC/PVA/0.5Fe-SRF were highlighted. For convenience, in the subsequent sensitivity calculations, the average price of the feedstock was taken to be used for the calculations with the highest and lowest prices of this raw material. In Fig. 6b, the cost of fertilizer production was most sensitive to fluctuations in tea leaf prices, resulting in a fluctuation of ±US$39.69. Subsequently, price fluctuations in compound NPK fertilizers, RSBC, and zeolite led to changes in the cost of CMC/PVA/0.5Fe-SRF production of ±US$27.16, ±US$12.53 and ±US$4.81, respectively.

The results of the pot tests showed that the nitrogen utilization efficiency (NUE) of tomatoes treated with CMC/PVA/0.5Fe-SRF was 1.21 times that of the NPK compound fertilizer. Improving the NUE led to a reduction in the demand for synthetic nitrogen fertilizers, which was an effective strategy for reducing GHG emissions from nitrogen fertilizer (Gao and Cabrera Serrenho 2023). There were five main sources of greenhouse gas emissions during the use of synthetic nitrogen fertilizers. The by-product N_2O was directly generated during the nitrification and denitrification processes by soil bacteria (Coskun et al. 2017; Qiao et al. 2015). The N_2O released by synthetic nitrogen fertilizers was produced indirectly through nitrate leaching and ammonia volatilization. Some of the ammonia gas emitted during these processes was converted into N_2O by soil bacteria (Pan et al. 2016). Furthermore, the urea and ammonium bicarbonate applied to the fields decomposed to produce CO_2. Additionally, the use of lime to neutralize soil acidification caused by nitrogen fertilizers also generated CO_2.

We established three conditions for conducting the subsequent calculation of GHG emissions. Condition 1 considered only the nitrogen in the NPK compound fertilizer, assuming that all the nitrogen was in the form of ammonium nitrate. Condition 2 divided the world into 10 regions to calculate GHG. Condition 3 specified that the data used in the calculation were based on the nitrogen fertilizer consumption reported by the International Fertilizer Association (IFA) for the year 2022 (https://www.ifastat.org/databases/plant-nutrition). Due to the assumption set in condition 1, the NPK compound fertilizer did not include urea or ammonium bicarbonate forms of nitrogen. As a result, the CO_2 emissions from the decomposition of these substances were not considered. As shown in Fig. 6e, when CMC/PVA/0.5Fe-SRF was used as a substitute, the nitrogen demand for NPK compound fertilizer could be reduced. Table S3 shows the nitrogen consumption in NPK compound fertilizers across regions, along with the reduced nitrogen demand assuming that CMC/PVA/0.5Fe-SRF were used as a substitute. Notably, under the fertilizer substitution scenario, using CMC/PVA/0.5Fe-SRF instead of traditional NPK compound fertilizers significantly reduced GHG emissions. As shown in Fig. 6d, e, the CMC/PVA/0.5Fe-SRF substitution intervention could reduce GHG emissions in East Asia by up to 17.77 Mt CO_2e. Other regions, such as West Europe, North America, and Latin America, respectively reduced their GHG missions by 0.77 Mt CO_2e, 0.53 Mt CO_2e, and 0.54 Mt CO_2e. To sum up, this demonstrated the economic feasibility of CMC/PVA/0.5Fe-SRF and evaluated their potential as an intervention to reduce GHG emissions.

4 Conclusion

This study developed a sustainable slow-release fertilizer by incorporating green-synthesized tea-extract iron nanoparticles into CMC/PVA coatings for zeolite–biochar hybrid cores. The engineered system achieved controlled nutrient release and micronutrient supplementation, significantly enhancing tomato growth, root development, soil water retention, and nutrient retention under controlled conditions. Soil analyses indicated improved cation exchange capacity, organic matter content, and balanced phosphorus availability, while an economic assessment confirmed cost-competitiveness and substantial potential for greenhouse gas mitigation through improved nitrogen use efficiency. These findings highlight the scalability and environmental value of integrating bio-based materials with functional nanotechnology

for modern agriculture. Despite the promising results obtained under controlled conditions, this study is limited by its short-term and small-scale scope. Future work will focus on extensive field-scale validation and in-depth analysis of long-term impacts on soil–microbe interactions to ensure sustainable application.

Supplementary Information

The online version contains supplementary material available at https://doi.org/10.1007/s42773-026-00592-1.

Additional file 1.

Acknowledgements
Not applicable.

Author contributions
Mengqiao Wu and Zefeng Ruan: Investigation, Methodology, Data curation, Visualization, Writing—original draft; Yuyuan Wu, Yang Cheng, Yuting Hong, Qinglin Gu, Yiting Zhang, Jialin Wei, Xiaowen Zhang, Chang Dong, and Xu Zhao: Investigation, Data curation; Yongfu Li: Writing—review & editing, Methodology, Validation; Chengfang Song and Bing Yu: Conceptualization, Supervision, Methodology, Supervision, Writing—review & editing, Validation, Project administration. The author(s) read and approved the final manuscript.

Funding
This work was financially supported by the National Key Research and Development Program of China (2022YFE0127800); the Key Research and Development Project of Science and Technology Department of Zhejiang Province (2023C02019; 2025C02096); the Zhejiang Province's "Three Rural and Nine Directions" Science and Technology Collaboration Plan (2024SNJF065).

Availability of data and materials
The datasets used or analyzed during the current study will be made available on request.

Declarations

Competing interests
The authors declare that they have no known competing financial interests or personal relationships that might have appeared to influence the work reported in this paper.

Author details
[1]Sino-Spain Joint Laboratory for Agricultural Environment Emerging Contaminants of Zhejiang Province, Zhejiang A&F University, Hangzhou 311300, China. [2]Fujian Key Laboratory of Functional Marine Sensing Materials, College of Material and Chemical Engineering, Minjiang University, Fuzhou 350108, China.

Received: 24 July 2025 Revised: 5 February 2026 Accepted: 21 February 2026
Published online: 24 March 2026

References

Adepu S, Khandelwal M (2020) Ex-situ modification of bacterial cellulose for immediate and sustained drug release with insights into release mechanism. Carbohydr Polym 249:116816
Buendia E, Tanabe K, Kranjc A, Baasansuren J, Fukuda M, Ngarize S, Osako A, Pyrozhenko Y, Shermanau P, Federici S (2019) Refinement to the 2006 IPCC guidelines for national greenhouse gas inventories, vol 5. IPCC, Geneva, p 194
Channab B-E, El Idrissi A, Ammar A, Akil A, White JC, Zahouily M (2024) ZIF-8 metal organic framework, carboxymethylcellulose and polyvinyl alcohol bio-nanocomposite controlled-release phosphorus fertilizer: improved P management and tomato growth. Chem Eng J 495:153610
Chen M, Wang F, Zhang D-l, Yi W-m, Liu Y (2021) Effects of acid modification on the structure and adsorption NH_4^+-N properties of biochar. Renew Energy 169:1343–1350
Chen Z, Liu T, Dong JF, Chen G, Li Z, Zhou JL, Chen Z (2023) Sustainable application for agriculture using biochar-based slow-release fertilizers: a review. ACS Sustain Chem Eng 11(1):1–12
Cheng Y, Wu M, Lu J, Zhang Y, Lu R, Li Y, Cai Y, Xiang H, Zhuang Z, Qiu Z (2024) Optimizing fabrication of coated fertilizers integrated with biochar for enhanced slow-release properties: mechanisms and cost-effectiveness analysis. Ind Crop Prod 222:120077
Coskun D, Britto DT, Shi W, Kronzucker HJ (2017) Nitrogen transformations in modern agriculture and the role of biological nitrification inhibition. Nat Plants 3(6):1–10
Costa P, Lobo JMS (2001) Modeling and comparison of dissolution profiles. Eur J Pharm Sci 13(2):123–133
Devatha C, Thalla AK, Katte SY (2016) Green synthesis of iron nanoparticles using different leaf extracts for treatment of domestic waste water. J Clean Prod 139:1425–1435
Diao F-M, Chen M-L, Tong L-Y, Chen Y-N, Diao Z-H (2023) A green synthesized medicine residue carbon-based iron composite for the removal of chromium (VI) and cadmium (II): performance, kinetics and mechanism. Environ Sci Pollut Res 30(35):84011–84022
Dong J, Liu Q, Yu L, Subhonqulov S (2021) The interaction mechanism of Fe^{3+} and NH_4^+ on chalcopyrite surface and its response to flotation separation of chalcopyrite from arsenopyrite. Sep Purif Technol 256:117778
Dong H, Tang S, Zhang L, Tong Z, Wu Z, Zhan P, Shao L, Qing Y, Liu J (2023) Wood-derived bio-coating materials incorporating hydrophobic lignin and hierarchically porous biochar for high-efficiency coating slow-release fertilizers. Int J Biol Macromol 242:124769
Dong C, Cheng Y, Wu M, Wang Q, Zhang Y, White JC, Xiang H, Cai Y, Li Y, Yu B (2025) Nanozeolite-coupled biochar-based controlled-release phosphorus fertilizer: performance, release mechanism, and techno-economic analysis. ACS Sustain Chem Eng 13(9):3785–3796
Gao Y, Cabrera Serrenho A (2023) Greenhouse gas emissions from nitrogen fertilizers could be reduced by up to one-fifth of current levels by 2050 with combined interventions. Nat Food 4(2):170–178
Gao Y, Fang Z, Van Zwieten L, Bolan N, Dong D, Quin BF, Meng J, Li F, Wu F, Wang H (2022) A critical review of biochar-based nitrogen fertilizers and their effects on crop production and the environment. Biochar 4(1):36
Goldsmith SB, Eon RS, Lapszynski CS, Badura GP, Osgood DT, Bachmann CM, Tyler AC (2020) Assessing salt marsh vulnerability using high-resolution hyperspectral imagery. Remote Sens 12(18):2938
Han X, Ma P, Shen M, Wen H, Xie J (2023) Modified porous starches loading curcumin and improving the free radical scavenging ability and release properties of curcumin. Food Res Int 168:112770
He H, Wu D, Wang Q, Luo C, Duan N (2016) Sequestration of hexavalent chromium by Fe (II)/Fe (III) hydroxides: structural Fe (II) reactivity and PO_4^{3-} effect. Chem Eng J 283:948–955
Huang Y, Lee X, Grattieri M, Yuan M, Cai R, Macazo FC, Minteer SD (2020) Modified biochar for phosphate adsorption in environmentally relevant conditions. Chem Eng J 380:122375
Jha VK, Hayashi S (2009) Modification on natural clinoptilolite zeolite for its NH_4^+ retention capacity. J Hazard Mater 169(1–3):29–35
Kassem I, Ablouh E-H, El Bouchtaoui F-Z, Hannache H, Ghalfi H, Sehaqui H, El Achaby M (2022) Cellulose nanofibers/engineered biochar hybrid materials as biodegradable coating for slow-release phosphate fertilizers. ACS Sustain Chem Eng 10(46):15250–15262
Kumar JA, Krithiga T, Manigandan S, Sathish S, Renita AA, Prakash P, Prasad BN, Kumar TP, Rajasimman M, Hosseini-Bandegharaei A (2021) A focus to green synthesis of metal/metal based oxide nanoparticles: various mechanisms and applications towards ecological approach. J Clean Prod 324:129198
Kumar V, Kaushik NK, Tiwari SK, Singh D, Singh B (2023) Green synthesis of iron nanoparticles: sources and multifarious biotechnological applications. Int J Biol Macromol 253:127017

Li Y, Zhao C (2017) Enhancing water oxidation catalysis on a synergistic phosphorylated NiFe hydroxide by adjusting catalyst wettability. ACS Catal 7(4):2535–2541
Li M, Zhao X, Cheng Y, Wu M, Dong C, Xiang H, Li Y, Cai Y, Zhang Z, Yu B (2025) Zinc oxide nanoparticles coupled biochar-based slow-release fertilizer for enhanced nutrient efficiency and sustainable agriculture. Ind Crops Prod 232:121265
Liang L, Sun W, Guan X, Huang Y, Choi W, Bao H, Li L, Jiang Z (2014) Weak magnetic field significantly enhances selenite removal kinetics by zero valent iron. Water Res 49:371–380
Lu J, Li Y, Cai Y, Jiang P, Yu B (2023) Co-incorporation of hydrotalcite and starch into biochar-based fertilizers for the synthesis of slow-release fertilizers with improved water retention. Bcha 5(1):44
Lu J, Wu M, Luo L, Lu R, Zhu J, Li Y, Cai Y, Xiang H, Song C, Yu B (2025) Incorporating iron oxide nanoparticles in polyvinyl alcohol/starch hydrogel membrane with biochar for enhanced slow-release properties of compound fertilizers. Carbohydr Polym 348:122834
Nayak P, Nandipamu TMK, Chaturvedi S, Dhyani V, Chandra S (2024) Synthesis, properties, and mechanistic release-kinetics modeling of biochar-based slow-release nitrogen fertilizers and their field efficacy. J Soil Sci Plant Nutr 24(4):7460–7479
Öğütveren ÜB, Öğütveren M (2017) Green synthesis of iron nano-materials by plants and their use in removal of pollutants from wastewaters–a review. Desalin Water Treat 78:141–154
Otero GS, Pascucci B, Branda MM, Miotto R, Belelli PG (2016) Evaluating the size of Fe nanoparticles for ammonia adsorption and dehydrogenation. Comput Mater Sci 124:220–227
Pan B, Lam SK, Mosier A, Luo Y, Chen D (2016) Ammonia volatilization from synthetic fertilizers and its mitigation strategies: a global synthesis. Agric Ecosyst Environ 232:283–289
Qiao C, Liu L, Hu S, Compton JE, Greaver TL, Li Q (2015) How inhibiting nitrification affects nitrogen cycle and reduces environmental impacts of anthropogenic nitrogen input. Glob Change Biol 21(3):1249–1257
Qu J, Che T, Shi L, Lu Q, Qi S (2019) A novel magnetic silica supported spinel ferrites NiFe2O4 catalyst for heterogeneous Fenton-like oxidation of Rhodamine B. Chin Chem Lett 30(6):1198–1203
Shaghaleh H, Hamoud YA, Xu X, Wang S, Liu H (2022) A pH-responsive/sustained release nitrogen fertilizer hydrogel based on aminated cellulose nanofiber/cationic copolymer for application in irrigated neutral soils. J Clean Prod 368:133098
Shahzad R, Koerniati S, Harlina PW, Hastilestari BR, Djalovic I, Prasad PV (2025) Iron oxide nanoparticles enhance alkaline stress resilience in bell pepper by modulating photosynthetic capacity, membrane integrity, carbohydrate metabolism, and cellular antioxidant defense. BMC Plant Biol 25(1):170
Sun H, Zhou Q, Zhao L, Wu W (2021) Enhanced simultaneous removal of nitrate and phosphate using novel solid carbon source/zero-valent iron composite. J Clean Prod 289:125757
Tang X, Li JH, Yang JY, Xiang ZC, He YY, Huang YZ, Zhou N, Luo W, Zhou Z (2025) Agricultural sustainability: biochar and bio-based polyurethane coupling coating to prepare novel controlled-release fertilizers. Ind Crop Prod 223:120296
Therby-Vale R, Lacombe B, Rhee SY, Nussaume L, Rouached H (2022) Mineral nutrient signaling controls photosynthesis: focus on iron deficiency-induced chlorosis. Trends Plant Sci 27(5):502–509
Tyagi V, Thakur A (2023) Carboxymethyl cellulose-polyvinyl alcohol based materials: a review. Mater Today.
Wang T, Su J, Jin X, Chen Z, Megharaj M, Naidu R (2013) Functional clay supported bimetallic nZVI/Pd nanoparticles used for removal of methyl orange from aqueous solution. J Hazard Mater 262:819–825
Wang T, Lin J, Chen Z, Megharaj M, Naidu R (2014) Green synthesized iron nanoparticles by green tea and Eucalyptus leaves extracts used for removal of nitrate in aqueous solution. J Clean Prod 83:413–419
Wang J, Xie H, Wu J, He W, Zhang X, Huang J, Feng Y, Xue L (2024) Fe/BC co-conditioners with environmental and economic benefits on composting: reduced NH3 emissions and improved fertilizer quality. Biochar 6(1):4
Wu Z, Su X, Lin Z, Owens G, Chen Z (2019) Mechanism of As (V) removal by green synthesized iron nanoparticles. J Hazard Mater 379:120811
Wu M, Lu J, Zhang Y, Ling Z, Lu R, Zhu J, Li Y, Cai Y, Xiang H, Zhang Z (2025) Chitosan hydrogel membrane embedded by metal-modified biochars for slow-release fertilizers. Int J Biol Macromol 306:141296
Xiang H, Yang J, Cao X, Wang N (2022) Flexible and highly sensitive triboelectric nanogenerator with magnetic nanocomposites for cultural heritage conservation and human motion monitoring. Nano Energ 101:107570
Xiao Y, Zhang Z, Lin J, Chen W, Huang J, Chen Z (2025) Machine learning predicts selectivity of green synthesized iron nanoparticles toward typical contaminants: critical factors in synthesis conditions, material properties, and reaction process. Environ Res 277:121605
Xu X, Weng X, Owens G, Chen Z (2024) Iron nanoparticles synthesized using *Euphorbia cochinchinensis* leaf extracts exhibited highly selective recovery of rare earth elements from mining wastewater: exploring the origin of high selectivity. J Hazard Mater 480:136320
Xu J, Ren C, Zhang X, Wang C, Wang S, Ma B, He Y, Hu L, Liu X, Zhang F (2025) Soil health contributes to variations in crop production and nitrogen use efficiency. Nat Food 6:507–609
Yang W, Sun Y, Yang F, Wang Y, Li X, Yang Y, Jiang D (2025) Preparation and properties of slow-release fertilizer containing urea encapsulated by pinecone biochar and cellulose acetate. Int J Biol Macromol 315:144448
Zhan L, You Y, Zhao L, Hao N, Bate B (2023) A study on the competitive adsorption process of NH^{4+} and Zn^{2+} on activated carbon and zeolite. Int J Environ Sci Technol 20(6):6039–6052
Zhang G, Liu H, Liu R, Qu J (2009) Removal of phosphate from water by a Fe–Mn binary oxide adsorbent. Colloid Interface Sci 335(2):168–174
Zhou J, Tang C, Vancov T, Fu S, Fang Y, Ge T, Dong Y, Luo Y, Yu B, Cai Y, White J, Li Y (2026) Biochar mitigates the suppressive effects of nitrogen deposition on soil methane uptake in a subtropical forest. Agric Ecosyst Environ 395:109951
Zhou J, Delgado-Baquerizo M, Vancov T, Liu Y, Zhou X, Chen J, Fang Y, Liu S, Yu B, Zhou G (2025a) Biochar mitigates nitrogen deposition-induced enhancement of soil N_2O emissions in a subtropical forest. Biol Fert Soils, 1–15.